The Journal of Chemical Physics

RESEARCH ARTICLE | OCTOBER 22 2024

Double Mpemba effect in the cooling of trapped colloids

Isha Malhotra ; Hartmut Löwen

J. Chem. Phys. 161, 164903 (2024)
https://doi.org/10.1063/5.0225749

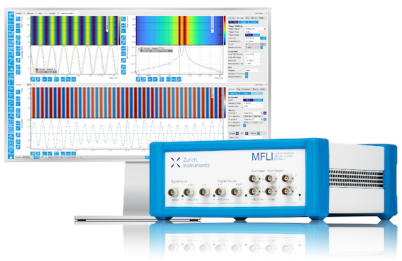

The Journal of Chemical Physics ARTICLE pubs.aip.org/aip/jcp

Double Mpemba effect in the cooling of trapped colloids

Cite as: J. Chem. Phys. 161, 164903 (2024); doi: 10.1063/5.0225749
Submitted: 26 June 2024 • Accepted: 4 October 2024 •
Published Online: 22 October 2024

Isha Malhotra[a] and Hartmut Löwen

AFFILIATIONS

Institut für Theoretische Physik II: Weiche Materie, Heinrich-Heine-Universität Düsseldorf, 40225 Düsseldorf, Germany

[a]Author to whom correspondence should be addressed: Isha.Malhotra@hhu.de

ABSTRACT

The Mpemba effect describes the phenomenon that a system at hot initial temperature cools faster than at an initial warm temperature in the same environment. Such an anomalous cooling has recently been predicted and realized for trapped colloids. Here, we investigate the freezing behavior of a passive colloidal particle by employing numerical Brownian dynamics simulations and theoretical calculations with a model that can be directly tested in experiments. During the cooling process, the colloidal particle exhibits multiple non-monotonic regimes in cooling rates, with the cooling time decreasing twice as a function of the initial temperature—an unexpected phenomenon we refer to as the Double Mpemba effect. In addition, we demonstrate that both the Mpemba and Double Mpemba effects can be predicted by various machine-learning methods, which expedite the analysis of complex, computationally intensive systems.

I. INTRODUCTION

The Mpemba effect challenges conventional understanding by proposing that hot water can cool and freeze faster than its cooler counterpart, contrary to intuitive expectations.[1] Despite extensive experimental investigations into this phenomenon in water, a consensus regarding its underlying cause remains elusive.[2–7] Recent research advances have demonstrated that the Mpemba effect is not limited to the freezing of water but occurs in a variety of contexts. This phenomenon has been identified in granular gases,[8–13] inertial suspensions,[14] Markovian models,[15–18] optical resonators,[19] molecular gases in contact with a thermal reservoir,[20,21] spin glasses,[22] and quantum systems.[23–32] Notably, it has also been observed in colloidal particle systems undergoing rapid thermal quenching.[33,34] In its simplest form, single particles are confined within one-dimensional asymmetric double-well potential, replicating the liquid and frozen states of water. The synthesis of experimental findings and theoretical insights, unravel the mechanisms driving this intriguing effect,[15,35,36] thereby advancing our comprehension of its fundamental principles.

In this study, we examine the cooling process of a trapped colloid within an asymmetric potential featuring a steep linear confinement, as shown in Fig. 1(a), and discover that it exhibits a pronounced Mpemba effect, occurring not just once but twice if the initial temperature is varied [Figs. 1(b) and 1(c)]—a phenomenon that is called as *Double Mpemba effect*. This effect has been previously observed in classical systems of inertial suspensions,[14] quantum systems,[37,38] and in other Markovian models.[16,39] However, to the best of our knowledge, the Double Mpemba effect has not been reported before for trapped colloids.

Furthermore, we explore how imposed bath temperatures influence the type of Mpemba—normal or Double—that the system exhibits. We have generalized a simple theoretical framework proposed by Kumar and Bechhoefer[33] that explains the observations of numerical simulations and quantitatively agrees with the analysis based on the eigenfunction expansion of the Fokker–Planck equation.[15,33,34,40]

Furthermore, traditional experimental and computational approaches to studying the Mpemba effect often face challenges due to the complexity and variability of the parameters involved. Specifically, predicting the type of Mpemba effect requires calculating cooling times across various initial temperatures or determining eigenvectors, both of which are computationally intensive. To overcome these challenges, we propose a novel approach that leverages theoretical modeling and machine learning[41–44] to predict the colloidal Mpemba effect with high accuracy. Amorim *et al.*[41] have also shown that machine-learning methods, such as decision trees, neural networks, and regression techniques, can accurately predict the Mpemba effect in complex systems such as the Ising model without explicit eigenvector calculations.

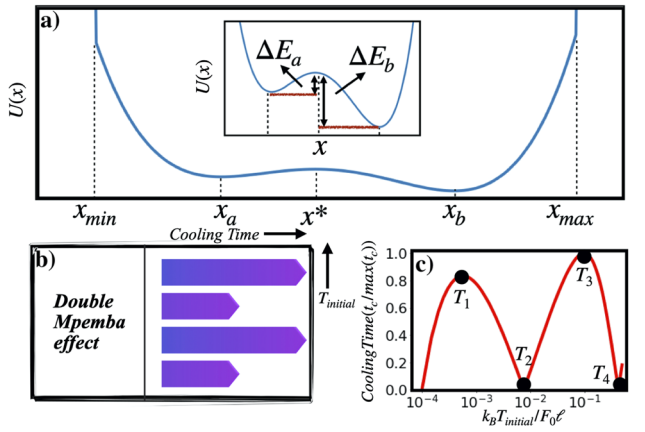

FIG. 1. (a) Schematic of the asymmetric potential $U(x)$ with a steep linear confinement beyond $x_{\min}$ and $x_{\max}$, potential minima at x_a and x_b, and a maximum at x^*. The inset shows the energy barriers ΔE_a and ΔE_b for the potential minima at x_a and x_b, respectively. (b) Double Mpemba effect, where each colored arrow represents a cooling process and the arrow's length depicts the time the system needs to cool down. (c) Cooling time t_c as a function of initial temperature to a fixed bath temperature $k_B T_{bath} = 10^{-4} F_0 \ell$. [Parameters: $x_{\min} = -0.25\ell$, $x_{\max} = 0.75\ell$, $F_1 = 6 \times 10^{-5} F_0 \ell$].

To illustrate the Mpemba effect, imagine two systems with temperatures ranging from warm to hot. Typically, when these systems are cooled to a set cold bath temperature, we would expect that the hotter the system, the longer it would take to cool. However, the Mpemba effect occurs when the hot system cools faster than the warm one. In the context of a passive colloid in an asymmetrical potential, this phenomenon arises because the hot particle possesses enough residual energy—defined as the mean potential energy after the system has begun cooling—to overcome potential barriers more effectively. This allows the hot particle to quickly settle into the cold state. In contrast, a warm particle, having less residual energy, struggles to cross the barrier, resulting in a slower cooling process. We show the existence of the Double Mpemba effect and that the key factors influencing the Mpemba effect are not only the residual energy but also the initial state of the system and the final bath temperature T_{bath}. This finding broadens our understanding of the Mpemba effect and highlights the complexity of cooling dynamics in these systems.

II. MODEL AND SIMULATION TECHNIQUE

We explore the process of cooling for a Brownian colloidal particle confined within a double-well potential through numerical simulations. The symmetry of the double-well potential is broken either by bringing a tilt in the potential or by the asymmetric placement of the potential in a domain [see Fig. 1(a)]. The motion of the Brownian particle, experiencing fluctuations at temperature T and undergoing overdamped motion, is described in one spatial dimension by Langevin equation,

$$\frac{dx}{dt} = -\frac{1}{\gamma}\partial_x U(x) + \eta(t), \tag{1}$$

where $\eta(t)$ represents the Gaussian white noise with zero mean and variance $\langle \eta(t)\eta(t') \rangle = 2D_T\delta(t-t')$. Here, the noise strength corresponds to the translational diffusion constant D_T of the particle, which is determined by the temperature T, given by the Stokes–Einstein relation $D_T = \frac{k_B T_{bath}}{\gamma}$, where k_B denotes the Boltzmann constant and γ represents the friction coefficient. The particle is subjected to an external double-well potential, similar to that described in Refs. 34 and 45, as shown in Fig. 1(a), and defined as follows:

$$U(x) = \begin{cases} -F_0 x + \kappa, & \text{if } x < x_{\min}, \\ F_1\left[\left(1 - \frac{x^2}{\alpha^2}\right)^2 - \frac{1}{2}\frac{x}{\alpha}\right], & \text{if } x_{\min} < x < x_{\max}, \\ F_0 x + \kappa_1, & \text{if } x > x_{\max}. \end{cases} \tag{2}$$

The components in Eq. (2) that scale with F_0 signify the presence of a linear potential with a slope corresponding to the maximum force that can be achieved experimentally,[33] while the component proportional to F_1 describes an asymmetric potential featuring two minima at x_a and x_b of varying heights and a maximum at x^*. The constants κ and κ_1 ensure the continuity of the potential at $x = x_{\min}$ and $x = x_{\max}$.

The length of the confining box denoted as $\ell = |x_{\max} - x_{\min}|$, serves as a convenient unit of length, and the parameter α is set to 0.125ℓ. When the length scale is combined with the translational diffusion constant, it yields a natural time scale expressed as $\tau_D = \frac{\ell^2}{D_T}$. Throughout this paper, the temperatures and energies are defined in units of $F_0\ell$ and γ is set to unity.

To gain quantitative insight into the relaxation process, we quantify the distance between the target equilibrium distribution $\pi_{\text{bath}}(x) \propto \exp(-U(x)/k_B T_{bath})$ and the probability distribution $P(x,t)$ during the cooling process. To find $P(x,t)$, we first generate the initial probability distribution $P(x, t=0) \propto \exp(-U(x)/k_B T_{initial})$ by performing 5000 independent simulation runs. For each run, we first equilibrate the system at temperature $T_{initial}$. Once equilibration is achieved, we record the particle's position. These recorded positions are then used to construct the initial probability distribution $P(x, t=0)$, representing the particle's equilibrium state at $T_{initial}$. Subsequently, we perform a rapid temperature quench to a bath temperature T_{bath}. For each of the 5000 independent runs, we quench the system to T_{bath} and allow the particle to equilibrate at this new temperature. After equilibration in each run, the particle's position is recorded. The data from these 5000 runs are then used to derive the final probability distribution $P(x,t)$, which reflects the particle's state at the bath temperature T_{bath}. Now, to construct the distance measure, we discretize the spatial components of both $\pi_{bath}(x)$ and $P(x,t)$ into N grid points, resulting in $\pi_{i,\text{bath}}$ and $P_i(t)$, respectively. The distance measure is then defined as

$$\mathscr{D}(t) = \frac{1}{N}\sum_{i=0}^{N} |P_i(t) - \pi_{i,\text{bath}}|. \tag{3}$$

From this measure, the cooling time t_c^{sim} can be determined. This is defined as the time when $\mathscr{D}(t)$ has decreased to the noise level, specified by $\sigma_{\mathscr{D}} = 0.01$, which accounts for the limitations imposed by the finite sample size (see Appendix C).

In the following, we present a theoretical formula by generalizing the approach proposed by Kumar and Bechhoefer[33] for calculating the cooling time scale of particles starting from various initial temperatures $T_{initial}$. The occupation ratios/probabilities $N_a(T)$ and $N_b(T)$, which indicate the probability of a particle in the left-hand domain $(-\infty, x^*)$ and right-hand domain (x^*, ∞), respectively, at a temperature T with $\beta = \frac{1}{k_B T}$ in equilibrium are given as

$$N_a(T) = \frac{\int_{-\infty}^{x^*} \exp\left(-\beta U(x)\right) dx}{\int_{-\infty}^{\infty} \exp\left(-\beta U(x)\right) dx}, \tag{4}$$

$$N_b(T) = 1 - N_a(T). \tag{5}$$

The time scale for cooling is approximately given as[46,47]

$$t_c \approx \tau_D |N_a(T_{initial}) - N_a(T_{bath})| \exp\left(\frac{\Delta E_i}{k_B T_{bath}}\right). \tag{6}$$

The Arrhenius-like exponential factor accounts for the diffusion over an energy barrier that a particle originally in the potential hole at x_a, will escape to x_b crossing the barrier at x^* [see Fig. 1(a)].[47–51] The expressions $\Delta E_a = U(x^*) - U(x_a)$ and $\Delta E_b = U(x^*) - U(x_b)$ define the energy barriers for the potential minima at x_a and x_b, respectively. Here, ΔE_i is equal to ΔE_a if $N_a(T_{initial}) > N_a(T_{bath})$; otherwise, it is equal to ΔE_b.

III. RESULTS

A. Cooling scenarios

In Fig. 1(c), we present the cooling curve calculated from the theory [see Eq. (6)] as a function of different initial temperatures. The cooling time t_c has a double minimum, indicating the presence of the Double Mpemba effect for our chosen parameters. The numerical simulations further confirm theoretical predictions where we calculate the distance measure $\mathscr{D}(t)$ as defined in Eq. (3) in Fig. 2. We show that particles at temperatures T_2 and T_4 cool very quickly, while particles at temperatures T_1 and T_3 take longer to relax, fully consistent with the theoretical calculations.

To understand the effect of different bath temperatures, we present the particle distribution and calculate the normalized cooling time from the theoretical model at various bath temperatures, as shown in Figs. 3(a) and 3(b), respectively. We observe that, at $T_{\text{bath}} = 5 \times 10^{-5} F_0 \ell$, the system exhibits the normal Mpemba effect, whereas at $T_{\text{bath}} = 10^{-4} F_0 \ell$, a strong Mpemba effect is observed. At $T_{\text{bath}} = 5 \times 10^{-4} F_0 \ell$, the cooling time shows double minima, indicating the presence of the Double Mpemba effect.

To validate the theoretical model and numerical simulations, we employ a recent approach that relates the Mpemba effect to an eigenvalue expansion.[15,34,35] The underlying probability density $P(x,t)$ of particle positions is given by the Fokker–Planck Equation (FPE) as

$$\frac{\partial P(x,t)}{\partial t} = -\frac{1}{\gamma}\frac{\partial}{\partial x}(F(x)P(x,t)) + \frac{k_B T_{bath}}{\gamma}\frac{\partial^2}{\partial x^2}P(x,t) \equiv \hat{L}P(x,t), \tag{7}$$

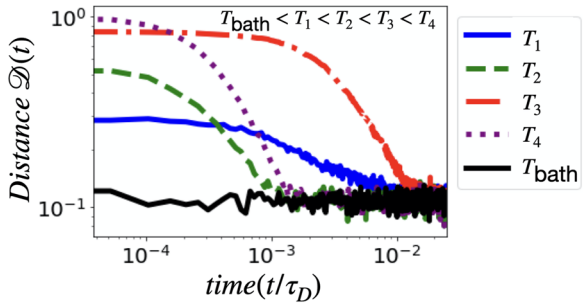

FIG. 2. Relaxation dynamics of the distance measure $\mathscr{D}(t)$ are examined by comparing the probability distributions of colloids at different initial temperatures: $k_B T_1 = 0.001 F_0 \ell$, $k_B T_2 = 0.007\,65 F_0 \ell$, $k_B T_3 = 0.1 F_0 \ell$, $k_B T_4 = 0.425 F_0 \ell$, and the probability distribution at the target bath temperature $k_B T_{bath} = 10^{-4} F_0 \ell$. For comparison, fluctuating numerical data for the distance are also shown when the system is *a priori* in the equilibrium cold state at bath temperature, which brings about a numerical noise level. These temperatures correspond to the points highlighted in Fig. 1(c), illustrating the Double Mpemba effect. Parameters are the same as in Fig. 1.

where $\hat{L}$ is the Fokker–Planck operator for Brownian motion and $F(x) = -\frac{\partial U(x)}{\partial x}$. The solution $P(x,t)$ of the FPE in terms of its eigenfunctions is given as

$$P(x,t) = \pi_{bath}(x) + \sum_{k=2}^{\infty} a_{k,ini} e^{-\lambda_k t} v_k(x). \tag{8}$$

The functions $v_k(x)$ are the kth right eigenfunction. They have an eigenvalue λ_k, ordered such that $\lambda_1 = 0 < \lambda_2 < \lambda_3 \cdots$. The coefficients $a_{k,ini}$ are real numbers dependent on the initial temperature and potential energy. Since λ_2 is smaller than λ_3, the higher-order terms become negligible, making λ_2 the slowest relaxation rate of the system. However, when $a_2 = 0$, the system relaxes much faster with $e^{-\lambda_3 t}$ leading to a strong Mpemba effect. In Fig. 3(c), we display the normalized $|a_2(T)|$ at different bath temperatures and demonstrate that the cooling behavior in Fig. 3(b) quantitatively agrees with $|a_2(T)|$. This shows that the cooling time at different initial temperatures is correlated to the second eigenvalue coefficient $|a_2(T)|$ of the Fokker–Planck equation. In Fig. 3(d), we illustrate the schematics of the variation of the cooling time plots for different types of Mpemba effects.

To understand the origin of different Mpemba effects, we examine the role of the first term defined in Eq. (6). In cases where the initial occupation probability matches the occupation probability at the final bath temperature, the particle relaxes very quickly as it does not need to cross the barrier to hop from the potential well at x_a to x_b, and vice versa. In Fig. 4(a), we show the occupation probability $N_a(T_{initial})$, which indicates the likelihood of a particle being in the right-hand domain (x^*, ∞) as a function of initial temperature $T_{initial}$. If for a given T_{bath}, $N_a(T_{initial}) = N_a(T_{bath})$, the particle immediately relaxes to the cold distribution, resulting in a pronounced Mpemba effect. Conversely, if $N_a(T_{initial}) \neq N_a(T_{bath})$, the particle must overcome the potential barrier to reach the equilibrium distribution at T_{bath}. Since crossing this barrier takes a considerable amount of time, the particle relaxes slowly. In Fig. 4(a), we observe that for the No Mpemba effect, $N_a(T_{initial})$ increases monotonically

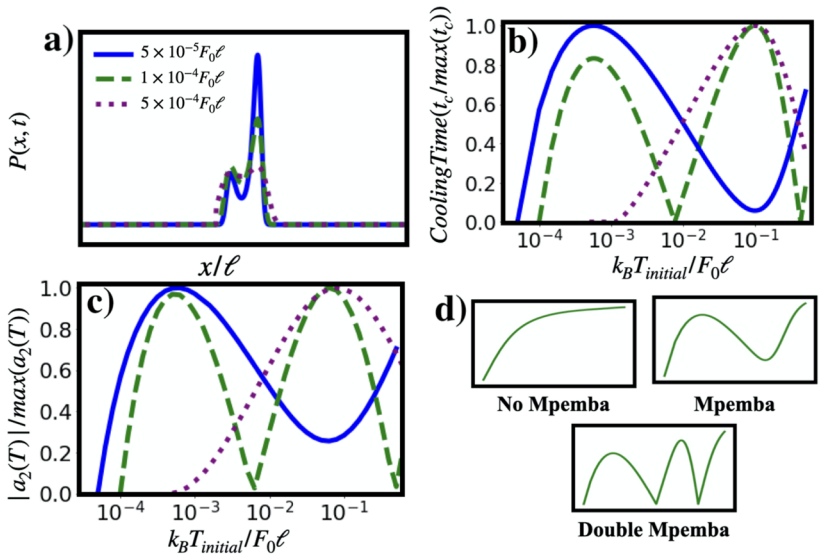

FIG. 3. (a) Probability distributions of colloidal particles at different k_BT_{bath} temperatures as indicated in the figure. (b) Cooling time normalized to [0, 1] by the maximum value of cooling time $[\max(t_c)]$ in the temperature range $5\times10^{-5}F_0\ell$ to $0.5\times F_0\ell$ as a function of initial temperature for different bath temperatures calculated from the theory. (c) The normalized second eigenvalue coefficient $\frac{|a_2(T)|}{\max(a_2(T))}$ as a function of the initial temperature $k_BT_{initial}$ is obtained by numerical calculations based on the Fokker Planck equation. (d) Schematics of the variation of cooling time as a function of initial temperature illustrating No Mpemba, Mpemba, and Double Mpemba effects. Parameters are the same as in Fig. 1.

with increasing temperature for the given parameters as indicated in the caption. This implies that hotter particles will take longer to relax to the cold distribution compared to warmer particles, indicating the absence of the Mpemba effect. Conversely, for the Double Mpemba effect, $N_a(T_{initial})$ exhibits non-monotonic behavior for a set of parameters mentioned in the caption. For the Double Mpemba effect, we observe that $N_a(T_{initial}) - N_a(T_{bath})$ has two nodes at T_2 and T_4, which signifies rapid transitions to the cold distribution occurring twice during the cooling process. In Fig. 4(b), we illustrate how the initial particle distributions result in the emergence of the Double Mpemba effect, where the slower relaxation occurs due to the necessity for particles at T_1 and T_3 to hop over the barrier in order to match the occupation probability at T_{bath}.

B. Machine learning for Mpemba classification

Finally, we employ machine learning (ML) to study the Mpemba effect, providing a faster and more efficient alternative to computationally intensive eigenvector or cooling time calculations across varying initial temperatures. By utilizing machine-learning algorithms, we can effectively classify and predict different Mpemba effect types based solely on observed data patterns. This allows us to bypass the need for direct simulation or analytical calculations for each new configuration.

1. Data generation and preprocessing

We first establish a comprehensive dataset based on the previously described theoretical model. The dataset includes the following input parameters: the minimum position $x_{\min}$, the maximum position $x_{\max}$, the bath temperature k_BT_{bath}, and the external force F_1. These parameters are systematically varied across a broad range of values to capture the full spectrum of potential behavior for the Mpemba effect,

$$\{x_{\min}, x_{\max}, k_BT_{bath}, F_1\} \rightarrow \begin{cases} 0 & \text{if No Mpemba,} \\ 1 & \text{if Mpemba,} \\ 2 & \text{if Double Mpemba.} \end{cases}$$

We vary $x_{\min}$ from -2.4ℓ to -0.125ℓ in intervals of 0.0625ℓ, and $x_{\max}$ from 0.625ℓ to 2.4ℓ in the same interval. The bath temperature k_BT_{bath} is varied from $5\times10^{-5}F_0\ell$ to $5\times10^{-4}F_0\ell$ in steps of $5\times10^{-5}F_0\ell$, and F_1 varies from $5\times10^{-5}F_0\ell$ to $5\times10^{-3}F_0\ell$ in steps of $5\times10^{-5}F_0\ell$. This careful, systematic variation ensures that the generated dataset, consisting of 780 000 data points, covers a diverse range of scenarios that represent the system's full complexity.

Before applying any machine-learning model, the dataset undergoes standard preprocessing steps. Each feature is normalized using a standard scalar to ensure uniform scaling. This normalization step is crucial because the algorithms we employ, particularly K-Nearest Neighbors (KNN)[52] and Logistic Regression,[53] rely on consistent feature scaling for effective performance. Without normalization, features with larger ranges could dominate others, leading to skewed predictions.

2. Model selection

We evaluate four different machine-learning algorithms to predict the occurrence and type of Mpemba effect: K-Nearest

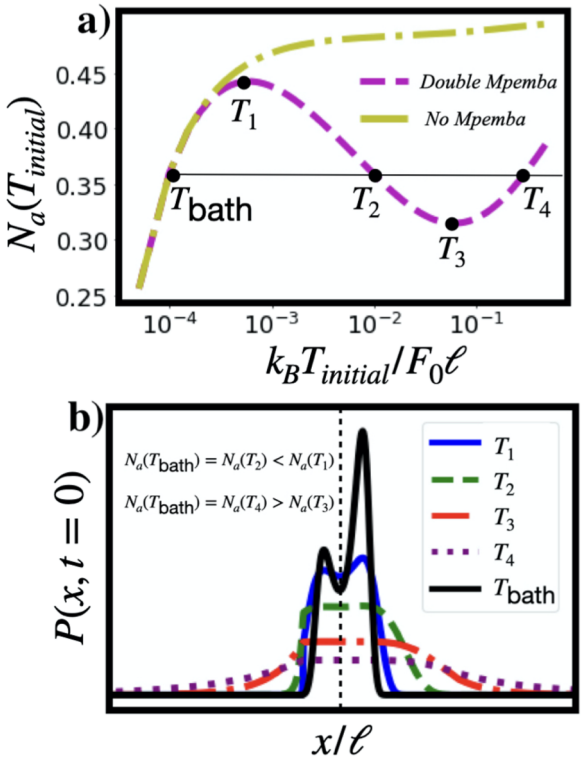

FIG. 4. (a) The occupation probability $N_a(T_{initial})$ as a function of temperature $T_{initial}$ for a system exhibiting No Mpemba [Parameters: $x_{min} = -0.5\ell$, $x_{max} = 0.5\ell$, $F_1 = 6 \times 10^{-5} F_0 \ell$] and Double Mpemba effect [Parameters: $x_{min} = -0.25\ell$, $x_{max} = 0.75\ell$, $F_1 = 6 \times 10^{-5} F_0 \ell$]. The temperatures T_1, T_2, T_3, and T_4 correspond to the temperatures mentioned in Fig. 2. (b) Initial probability distribution $P(x, t = 0)$ at temperatures T_1, T_2, T_3, and T_4 and $k_B T_{bath} = 10^{-4} F_0 \ell$ demonstrating that $N_a(T_{bath}) = N_a(T_2) < N_a(T_1)$ and $N_a(T_{bath}) = N_a(T_4) > N_a(T_3)$.

Neighbors (KNN),[52] Logistic Regression,[53] Decision Tree,[54] and Random Forest.[55]

3. K-nearest neighbors (KNN)

KNN is a non-parametric algorithm that classifies new data points based on the majority class among its closest neighbors in the feature space. We employ the Euclidean distance metric and test various values of k (the number of neighbors) to find the optimal setting. The inherent simplicity of KNN, combined with the benefits of feature scaling, makes it a valuable baseline model for classification.

4. Logistic regression

We utilize a one-vs-rest (OvR) strategy for multiclass classification, where each class is treated as a binary classification problem. The model is trained using the LBFGS solver, which is efficient for large datasets. Logistic regression serves as a linear model that can quickly identify separable classes, making it suitable for distinguishing between No Mpemba, Mpemba, and Double Mpemba effects when the decision boundaries are relatively simple.

5. Decision tree

To capture nonlinear relationships between features, we use a decision tree model with a maximum depth of 10. The decision tree, built using the entropy criterion, can identify complex patterns in the data by recursively partitioning the feature space. We limit the depth to avoid overfitting while ensuring that the tree has sufficient capacity to model the inherent complexity of the Mpemba effect.

6. Random forest

As an ensemble method, Random Forest combines the predictions of multiple decision trees (50 in this case) to improve overall accuracy and robustness. By averaging the predictions from multiple trees, Random Forest reduces the variance of individual decision trees and enhances the model's ability to generalize to unseen data. This method is especially useful in our study due to the complex and potentially overlapping parameter spaces of different Mpemba effect types.

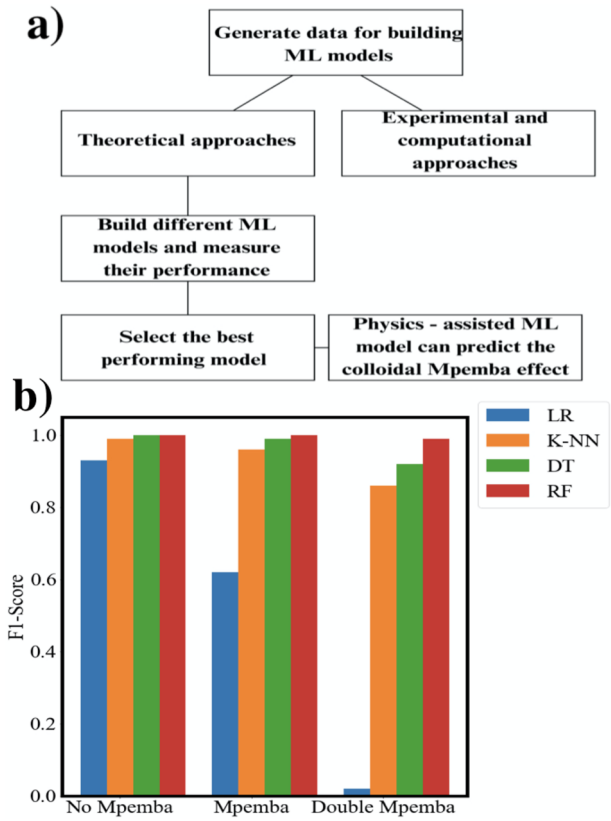

FIG. 5. (a) Overview of the methodology for predicting the Mpemba effect. The process begins with generating data for building machine-learning models either by theoretical or experimental/computational approaches. These data are used to build and evaluate multiple ML models. The performance of these models is assessed, and the best-performing model is selected. Finally, the selected physics-assisted machine-learning model is used to predict the colloidal Mpemba effect. (b) Calculated F1-score of different ML models in predicting No-Mpemba, Mpemba, and Double Mpemba.

7. Training and model evaluation

The dataset is split into a training set (70%) and a test set (30%) to train the models and evaluate their performance on unseen data. By using a test set that the models have not seen during training, we can more accurately assess their generalization abilities.

After preprocessing, we evaluate the models using the F1 score, a metric that balances precision and recall, providing a holistic measure of the model's performance. Precision refers to the proportion of correct positive predictions, while recall measures how many actual positives were correctly identified. This balance is essential given the potential imbalances between the occurrence of No Mpemba, Mpemba, and Double Mpemba cases in the dataset,

$$\text{F1 Score} = 2 \times \frac{\text{Precision} \times \text{Recall}}{\text{Precision} + \text{Recall}}.$$

As illustrated in Fig. 5(a), all four models are evaluated based on their F1 scores for each class (No Mpemba, Mpemba, Double Mpemba). Figure 5(b) demonstrates that the Random Forest consistently achieves the highest F1 scores across all Mpemba scenarios. Its ensemble nature, which aggregates the results of multiple trees, allows it to capture the complex relationships between features, leading to improved generalization and precise prediction compared to the other models. In contrast, while the Decision Tree and KNN models also perform well, they exhibit lower generalization due to either overfitting or limited flexibility in partitioning the feature space.

IV. CONCLUSIONS

We have investigated the influence of potential parameters and bath temperature on the manifestation of different types of Mpemba effects, demonstrating how these factors can fundamentally alter the relaxation process and lead to the Double Mpemba effect, characterized by a cooling trajectory with two minima. Furthermore, we generalized a simple theoretical framework that quantitatively aligns with the analysis based on the eigenfunction expansion of the Fokker–Planck equation.[33] In addition, we have integrated our theoretical model with advanced machine-learning techniques to enhance the predictability of this intriguing phenomenon.

Future research could explore the application of our findings to other systems exhibiting the Mpemba effect. It would be particularly interesting to examine how varying bath temperatures and different types of potentials affect the Mpemba effect in systems such as active colloids and many-particle systems. This model can also be used to study the Mpemba effect in quantum systems,[23,24] offering insights into the relaxation dynamics and thermal behaviors of complex quantum systems. A promising avenue for future research is to deepen our investigation into the Kovacs effect[56–60] using our model, to uncover the intricate dynamics and memory effects that influence the non-monotonic relaxation behavior in diverse physical systems.

Our results can be tested in real-space experiments of colloidal particles in an optical double-well potential.[33,61] To study the effect of different initial temperatures $T_{initial}$, the external potential has to be switched from one initial to another, which is proportional to the initial one.

ACKNOWLEDGMENTS

I.M. acknowledges the support from the Alexander von Humboldt Foundation. H.L. acknowledges the support from the Deutsche Forschungsgemeinschaft (DFG) within the Project No. LO 418/29.

AUTHOR DECLARATIONS

Conflict of Interest

The authors have no conflicts to disclose.

Author Contributions

Isha Malhotra: Conceptualization (equal); Data curation (equal); Formal analysis (equal); Funding acquisition (equal); Investigation (equal); Methodology (equal); Project administration (equal); Resources (equal); Software (equal); Validation (equal); Visualization (equal); Writing – original draft (equal); Writing – review & editing (equal). **Hartmut Löwen**: Conceptualization (equal); Data curation (equal); Formal analysis (equal); Funding acquisition (equal); Investigation (equal); Methodology (equal); Project administration (equal); Resources (equal); Software (equal); Supervision (lead); Validation (equal); Visualization (equal); Writing – original draft (equal); Writing – review & editing (equal).

DATA AVAILABILITY

The data that support the findings of this study are available from the corresponding author upon reasonable request.

APPENDIX A: CALCULATION OF EFFECTIVE TEMPERATURE $T_{effective}(t)$ FOR SYSTEMS GENERATED AT DIFFERENT INITIAL TEMPERATURES

We associate a time-dependent effective temperature $T_{effective}(t)$ with the probability distribution function $P(x,t)$ through a local equilibrium definition as

$$\int_{-\infty}^{\infty} dx\, U(x) P(x,t) = \frac{\int_{-\infty}^{\infty} dx\, U(x) e^{-\beta(t)U(x)}}{\int_{-\infty}^{\infty} dx\, e^{-\beta(t)U(x)}}. \tag{A1}$$

Here, $\beta(t) = \frac{1}{k_B T_{effective}(t)}$ represents the inverse temperature, and $U(x)$ is the potential energy function. The left-hand side of the equation represents the expectation value of the potential energy based on the probability distribution $P(x,t)$, while the right-hand side corresponds to the equilibrium expectation value of the potential energy at temperature $T_{effective}(t)$.

By solving this equation, we obtain a time-dependent temperature $T(t)$ that characterizes the system's instantaneous thermal state. This approach provides valuable insights into the dynamic thermal properties of the system as it evolves. In Fig. 6, we observe two instances where the initially hotter system surpasses the initially cooler system, both under the same T_{bath}. Particles starting at temperature T_2, which is higher than T_1, overtake those initially at

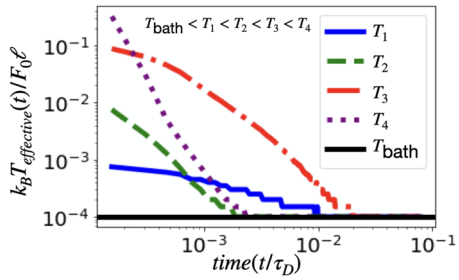

FIG. 6. Effective temperature $k_B T_{effective}$ as a function of time for particles generated at different initial temperatures $k_B T_1 = 0.001 F_0 \ell$, $k_B T_2 = 0.007\,65 F_0 \ell$, $k_B T_3 = 0.1 F_0 \ell$, and $k_B T_4 = 0.425 F_0 \ell$ taken to $k_B T_{bath} = 10^{-4} F_0 \ell$. Parameters are the same as in Fig. 1.

T_1. Similarly, particles at temperature T_4, which is higher than T_3, surpass those initially at T_3.

APPENDIX B: KULLBACK–LEIBLER DIVERGENCE

In this study, the Kullback–Leibler (KL) divergence[62] is also employed to quantify the differences in probability distributions, providing insights into the system's behavior. The KL divergence is calculated using the following equation:

$$\mathscr{D}_{KL} = \frac{1}{N}\sum_{i=1}^{N} P_i(t) \ln\left(\frac{P_i(t)}{\pi_{i,\text{bath}}}\right) \tag{B1}$$

In Fig. 7, we present both distance measures for the Double Mpemba effect based on the data shown in Fig. 2. This figure demonstrates that the observation of the Mpemba effect is independent of the chosen distance function, as the crossing of curves is consistently observed regardless of the distance measure used. Although the KL divergence provides quantitatively similar results to $\mathscr{D}(t)$ distance measure, it can become infinite when probability bins contain zero counts, necessitating the use of pseudo counts to regularize the equilibrium distribution.

APPENDIX C: COMPARISON OF THEORETICAL APPROACH AND NUMERICAL SIMULATIONS

Here, we present a comparison between the normalized cooling time t_c^{sim} derived from our numerical simulations and the normalized cooling time t_c calculated using Eq. (6). Figure 8(a) corresponds to the parameter set that exhibits the Double Mpemba effect, while Fig. 8(b) shows the single Mpemba effect. For the calculation of t_c^{sim}, we generated ten distributions for $P(x,t)$, each based on 5000 independent simulation runs. In each run, the system is quenched to the bath temperature T_{bath}, allowed to equilibrate, and then the particle's position is recorded. The data from these runs are used to construct the final probability distributions $P(x,t)$ for each of the ten sets, reflecting the particle's equilibrium state at T_{bath}. The cooling time t_c^{sim} is then measured by distance measure as mentioned in Sec. II. These two plots demonstrate a good agreement between the numerical simulations and the theoretical predictions.

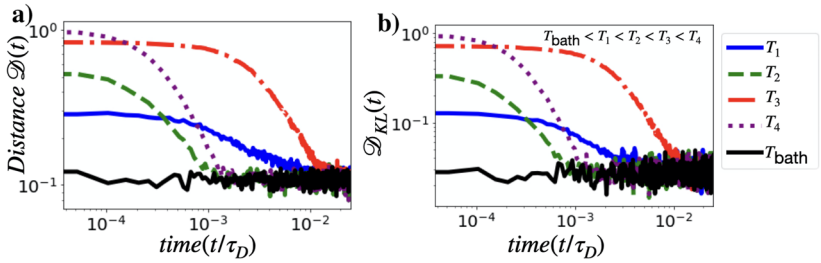

FIG. 7. "Distance" (a) $\mathscr{D}(t)$ and (b) $\mathscr{D}_{KL}(t)$ for temperatures $k_B T_1 = 0.001 F_0 \ell$, $k_B T_2 = 0.007\,65 F_0 \ell$, $k_B T_3 = 0.1 F_0 \ell$, and $k_B T_4 = 0.425 F_0 \ell$ taken to $k_B T_{bath} = 10^{-4} F_0 \ell$. The parameters are the same as in Fig. 1.

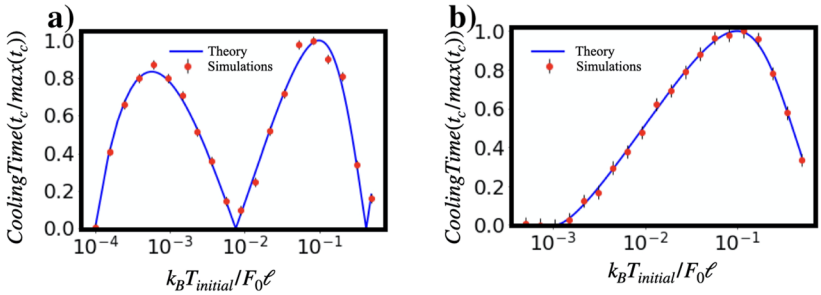

FIG. 8. Cooling time normalized to [0, 1] by the maximum value of cooling time [max(t_c) or max (t_c^{sim})] in the temperature range of $5 \times 10^{-5} F_0 \ell$ to $0.5 F_0 \ell$ as a function of initial temperature. The solid line shows the theoretical calculation and red data points are extracted from our simulation. (a) The bath temperature is $k_B T_{bath} = 10^{-4} F_0 \ell$. (b) The bath temperature is $k_B T_{bath} = 5 \times 10^{-4}$. Parameters are the same as in Fig. 1.

REFERENCES

[1] E. B. Mpemba and D. G. Osborne, "Cool?," Phys. Educ. **4**(3), 172–175 (1969).
[2] M. Jeng, "The Mpemba effect: When can hot water freeze faster than cold?," Am. J. Phys. **74**, 514–522 (2006).
[3] B. Wojciechowski, I. Owczarek, and G. Bednarz, "Freezing of aqueous solutions containing gases," Cryst. Res. Technol. **23**, 843–848 (1988).
[4] M. Vynnycky and N. Maeno, "Axisymmetric natural convection-driven evaporation of hot water and the Mpemba effect," Int. J. Heat Mass Transfer **55**, 7297–7311 (2012).
[5] M. Vynnycky and S. Kimura, "Can natural convection alone explain the Mpemba effect?," Int. J. Heat Mass Transfer **80**, 243–255 (2015).
[6] H. C. Burridge and P. F. Linden, "Questioning the Mpemba effect: Hot water does not cool more quickly than cold," Sci. Rep. **6**, 37665 (2016).
[7] D. Auerbach, "Supercooling and the Mpemba effect: When hot water freezes quicker than cold," Am. J. Phys. **63**, 882–885 (1995).
[8] A. Lasanta, F. Vega Reyes, A. Prados, and A. Santos, "When the hotter cools more quickly: Mpemba effect in granular fluids," Phys. Rev. Lett. **119**, 148001 (2017).
[9] A. Torrente, M. A. López-Castaño, A. Lasanta, F. V. Reyes, A. Prados, and A. Santos, "Large Mpemba-like effect in a gas of inelastic rough hard spheres," Phys. Rev. E **99**, 060901 (2019).
[10] A. Biswas, V. Prasad, O. Raz, and R. Rajesh, "Mpemba effect in driven granular Maxwell gases," Phys. Rev. E **102**, 012906 (2020).
[11] A. Biswas, V. Prasad, and R. Rajesh, "Mpemba effect in an anisotropically driven granular gas," Europhys. Lett. **136**, 46001 (2022).
[12] E. Mompó, M. A. López-Castaño, A. Lasanta, F. Vega Reyes, and A. Torrente, "Memory effects in a gas of viscoelastic particles," Phys. Fluids **33**, 062005 (2021).
[13] A. Megías and A. Santos, "Mpemba-like effect protocol for granular gases of inelastic and rough hard disks," Front. Phys. **10**, 971671 (2022).
[14] S. Takada, H. Hayakawa, and A. Santos, "Mpemba effect in inertial suspensions," Phys. Rev. E **103**, 032901 (2021).
[15] Z. Lu and O. Raz, "Nonequilibrium thermodynamics of the Markovian Mpemba effect and its inverse," Proc. Natl. Acad. Sci. U. S. A. **114**, 5083–5088 (2017).
[16] I. Klich, O. Raz, O. Hirschberg, and M. Vucelja, "Mpemba index and anomalous relaxation," Phys. Rev. X **9**, 021060 (2019).
[17] D. M. Busiello, D. Gupta, and A. Maritan, "Inducing and optimizing Markovian Mpemba effect with stochastic reset," New J. Phys. **23**, 103012 (2021).
[18] J. Lin, K. Li, J. He, J. Ren, and J. Wang, "Power statistics of Otto heat engines with the Mpemba effect," Phys. Rev. E **105**, 014104 (2022).
[19] T. Keller, V. Torggler, S. B. Jäger, S. Schütz, H. Ritsch, and G. Morigi, "Quenches across the self-organization transition in multimode cavities," New J. Phys. **20**, 025004 (2018).
[20] A. Santos and A. Prados, "Mpemba effect in molecular gases under nonlinear drag," Phys. Fluids **32**, 072010 (2020).
[21] A. Patrón, B. Sánchez-Rey, and A. Prados, "Strong nonexponential relaxation and memory effects in a fluid with nonlinear drag," Phys. Rev. E **104**, 064127 (2021).
[22] M. Baity-Jesi, E. Calore, A. Cruz, L. A. Fernandez, J. M. Gil-Narvión, A. Gordillo-Guerrero, D. Iñiguez, A. Lasanta, A. Maiorano, E. Marinari *et al.*, "The Mpemba effect in spin glasses is a persistent memory effect," Proc. Natl. Acad. Sci. U. S. A. **116**, 15350–15355 (2019).
[23] A. K. Chatterjee, S. Takada, and H. Hayakawa, "Quantum Mpemba effect in a quantum dot with reservoirs," Phys. Rev. Lett. **131**, 080402 (2023).
[24] A. Nava and M. Fabrizio, "Lindblad dissipative dynamics in the presence of phase coexistence," Phys. Rev. B **100**, 125102 (2019).
[25] F. Carollo, A. Lasanta, and I. Lesanovsky, "Exponentially accelerated approach to stationarity in Markovian open quantum systems through the Mpemba effect," Phys. Rev. Lett. **127**, 060401 (2021).
[26] S. K. Manikandan, "Equidistant quenches in few-level quantum systems," Phys. Rev. Res. **3**, 043108 (2021).
[27] F. Ares, S. Murciano, and P. Calabrese, "Entanglement asymmetry as a probe of symmetry breaking," Nat. Commun. **14**, 2036 (2023).
[28] F. Ivander, N. Anto-Sztrikacs, and D. Segal, "Hyperacceleration of quantum thermalization dynamics by bypassing long-lived coherences: An analytical treatment," Phys. Rev. E **108**, 014130 (2023).
[29] A. Nava and R. Egger, "Mpemba effects in open nonequilibrium quantum systems," Phys. Rev. Lett. **133**(13), 136302 (2024).
[30] S. Aharony Shapira, Y. Shapira, J. Markov, G. Teza, N. Akerman, O. Raz, and R. Ozeri, "Inverse Mpemba effect demonstrated on a single trapped ion qubit," Phys. Rev. Lett. **133**, 010403 (2024).
[31] S. Liu, H.-K. Zhang, S. Yin, and S.-X. Zhang, "Symmetry restoration and quantum Mpemba effect in symmetric random circuits," Phys. Rev. Lett. **133**(14), 140405 (2024).
[32] S. Liu, H.-K. Zhang, S. Yin, S.-X. Zhang, and H. Yao, "Quantum Mpemba effects in many-body localization systems," arXiv:2408.07750 (2024).
[33] A. Kumar and J. Bechhoefer, "Exponentially faster cooling in a colloidal system," Nature **584**, 64–68 (2020).
[34] F. J. Schwarzendahl and H. Löwen, "Anomalous cooling and overcooling of active colloids," Phys. Rev. Lett. **129**, 138002 (2022).
[35] J. Bechhoefer, A. Kumar, and R. Chétrite, "A fresh understanding of the Mpemba effect," Nat. Rev. Phys. **3**, 534–535 (2021).
[36] R. Chétrite, A. Kumar, and J. Bechhoefer, "The metastable Mpemba effect corresponds to a non-monotonic temperature dependence of extractable work," Front. Phys. **9**, 654271 (2021).
[37] A. K. Chatterjee, S. Takada, and H. Hayakawa, "Multiple quantum Mpemba effect: Exceptional points and oscillations," Phys. Rev. A **110**, 022213 (2024).
[38] K. Chalas, F. Ares, C. Rylands, and P. Calabrese, "Multiple crossing during dynamical symmetry restoration and implications for the quantum Mpemba effect," arXiv:2405.04436 (2024).
[39] A. Biswas and A. Pal, "Mpemba effect on non-equilibrium active Markov chains," arXiv:2403.17547 (2024).
[40] T. Sandev, A. Chechkin, H. Kantz, and R. Metzler, "Diffusion and Fokker-Planck-Smoluchowski equations with generalized memory kernel," Fractional Calculus Appl. Anal. **18**, 1006–1038 (2015).
[41] F. Amorim, J. Wisely, N. Buckley, C. DiNardo, and D. Sadasivan, "Predicting the Mpemba effect using machine learning," Phys. Rev. E **108**, 024137 (2023).
[42] P. Cunningham, M. Cord, and S. J. Delany, "Supervised learning," in *Machine Learning Techniques for Multimedia* (Springer, 2008), pp. 21–49.
[43] T. Hastie, R. Tibshirani, and J. Friedman, "Overview of supervised learning," in *The Elements of Statistical Learning: Data Mining, Inference, and Prediction* (Springer, 2009), pp. 9–41.
[44] L. Breiman, J. Friedman, R. Olshen, and C. Stone, *Classification and Regression Trees* (Wadsworth and Brooks, Monterey, CA, 1984).
[45] A. Kumar, R. Chétrite, and J. Bechhoefer, "Anomalous heating in a colloidal system," Proc. Natl. Acad. Sci. U. S. A. **119**, e2118484119 (2022).
[46] W. B. Russel, D. A. Saville, and W. R. Schowalter, *Colloidal Dispersions* (Cambridge University Press, 1991).
[47] S. Chandrasekhar, "Stochastic problems in physics and astronomy," Rev. Mod. Phys. **15**, 1–89 (1943).
[48] P. Hänggi, P. Talkner, and M. Borkovec, "Reaction-rate theory: Fifty years after Kramers," Rev. Mod. Phys. **62**, 251 (1990).
[49] P. Kraikivski, R. Lipowsky, and J. Kierfeld, "Barrier crossing of semiflexible polymers," Europhys. Lett. **66**, 763 (2004).
[50] A. Sharma, R. Wittmann, and J. M. Brader, "Escape rate of active particles in the effective equilibrium approach," Phys. Rev. E **95**, 012115 (2017).
[51] A. Scacchi, J. M. Brader, and A. Sharma, "Escape rate of transiently active Brownian particle in one dimension," Phys. Rev. E **100**, 012601 (2019).
[52] P. A. Devijver and J. Kittler, *Pattern Recognition: A Statistical Approach* (Prentice-Hall, London, 1982).
[53] J. S. Cramer, "The early origins of the logit model," Stud. Hist. Philos. Sci. Part C **35**, 613–626 (2004).
[54] J. R. Quinlan, "Induction of decision trees," Mach. Learn. **1**, 81–106 (1986).
[55] L. Breiman, "Random forests," Mach. Learn. **45**, 5–32 (2001).
[56] A. J. Kovacs, R. A. Stratton, and J. D. Ferry, "Dynamic mechanical properties of polyvinyl acetate in shear in the glass transition temperature range," J. Phys. Chem. **67**, 152–161 (1963).

[57]A. J. Kovacs, J. J. Aklonis, J. M. Hutchinson, and A. R. Ramos, "Isobaric volume and enthalpy recovery of glasses. II. A transparent multiparameter theory," J. Polym. Sci., Polym. Phys. Ed. **17**, 1097–1162 (1979).
[58]E. M. Bertin, J.-P. Bouchaud, J.-M. Drouffe, and C. Godrèche, "The Kovacs effect in model glasses," J. Phys. A: Math. Gen. **36**, 10701–10719 (2003).
[59]R. Kürsten, V. Sushkov, and T. Ihle, "Giant Kovacs-like memory effect for active particles," Phys. Rev. Lett. **119**, 188001 (2017).
[60]A. Santos, "Mpemba meets Newton: Exploring the Mpemba and Kovacs effects in the time-delayed cooling law," Phys. Rev. E **109**, 044149 (2024).
[61]I. Buttinoni, L. Caprini, L. Alvarez, F. J. Schwarzendahl, and H. Löwen, "Active colloids in harmonic optical potentials," Europhys. Lett. **140**, 27001 (2022).
[62]S. Kullback and R. Leibler, "On information and sufficiency," Ann. Math. Stat. **22**, 79–86 (1951).